Uncertainty Quantification of Conjugate Heat Transfer in Stratified Fluid Flow

Application of non-intrusive polynomial chaos

Project Report

IBM Research UK
STFC Hartree Centre

Title:
Uncertainty Quantification of Conjugate Heat Transfer in Stratified Fluid Flow

Theme:
Stochastic modelling

Participant(s):
Samuel Antão (IBM)
Eloisa Bentivegna (IBM)
Wendi Liu (STFC)
Charles Moulinec (STFC)
Robert Sawko (IBM)
Alex Skillen (STFC)*
Christopher Thompson (IBM)
Małgorzata Zimoń (IBM)*

Further Information:
If you would like further information about this report or to discuss its content, please contact:
*alex.skillen@stfc.ac.uk,
*malgorzata.zimon@uk.ibm.com

Date of Completion:
March 8, 2019

This work was supported by the STFC Hartree Centre's Innovation Return on Research programme, funded by the Department for Business, Energy & Industrial Strategy.

Contents

Executive Summary

Knowledge of a system's response to unknown operating conditions can be of key importance in engineering design. A standard engineering approach might involve performing a small handful of calculations to assess the influence of operating conditions on quantities of interest. However, this simple approach may provide an incomplete picture, potentially leading to poor design decisions. A brute-force approach (performing a large number of simulations, over a range of operating conditions) can provide a more complete mapping between inputs and outputs, but at a significant computational cost.

In this work we apply advanced uncertainty quantification techniques which allow us to maximise the knowledge extracted from the modelled system and, crucially, its response to uncertain input parameters. This is done without changing existing simulation codes. In the report, we show that we can perform such a study in a more efficient manner than the brute-force approach – at least 1-2 orders of magnitude less computational cost, with no loss in accuracy.

We demonstrate the use of these tools by assessing the propagation of thermal transients within a u-shaped bend. A hot-shock is introduced at the inlet, and allowed to propagate through the domain. This test-case is relevant to nuclear applications, where hot-cold cycles can lead to thermal fatigue and material failure. The influence shock-magnitude on wall temperatures (or wall stresses) is assessed. Rapid low-fidelity RANS (Reynolds-averaged Navier–Stokes) simulations, as typically used in industry, form the basis of the model.

The analysis we present shows a bi-modal response, in which extreme values of temperature within the pipe walls are more likely to occur than the mean value (despite a uniform distribution on the inlet shock-magnitude). Standard engineering practice may miss this as mean values are often focussed upon. The study reveals that the input-output-mapping for this flow is complex and requires novel approaches to efficiently determine the statistics.

In addition to the wall-temperatures, we also asses the thermally-induced stresses within the solid domain. We achieve this by coupling the Computational Fluid Dynamics (CFD) code with a Finite Element Method (FEM) code for stress analysis. A one-way coupling is performed, as solid displacements have an insignificant in-

fluence on the fluid-flow. This preliminary work is important as it will allow us to infer the likelihood of thermal fatigue (when coupled with an empirical fatigue model). For the test-case under consideration, stresses close to the yield-stress are observed, and hence thermal fatigue would be likely within only a few cycles.

Technical Report

Chapter 1

Introduction

Uncertainty quantification (UQ) is broadly defined as the study of errors associated with models, numerical algorithms and experiments. It is used to estimate the sensitivities of predicted outcomes or quantities of interest. Recently, a systematic UQ analysis of model input has emerged as an active area of research.

In this report we apply UQ in the context of an industrial computational fluid dynamics (CFD) study. Turbulent, thermally stratified flow in a U-shaped pipe has been selected as an example problem and models of varying fidelity were used. The choice has been motivated by the presence of complex physical mechanisms, transient nature of the flow and the presence of input uncertainties, all common to many industrial CFD scenarios.

Over the course of their lifetime pipelines in complex cooling and transport systems will experience numerous thermal transients of varying characteristics. The focus in this report is placed on forward propagation of model input uncertainties in order to capture the effect of these events in a statistical manner and thus provide engineers with a better representation of operating conditions. Using this type of analysis will lead to improved reliability and risk assessment.

The practical utility of UQ relies heavily on the ability to perform a certain number of model runs constraining significantly the choice of useful methods. The report details some available procedures with their associated computational costs giving a guideline on the application of UQ methodology for comparable studies.

The report is organised as follows. The simulation details are provided in Section 2. Section 3 gives the theory behind UQ method. In Section 4, the application and the uncertainty quantification procedure are described, followed by results and discussion. Finally, we draw some conclusions and discuss future work.

Chapter 2

Numerical modelling

The simulation is based upon that of Viollet [33].

2.1 Physical properties

The flow, thermal and material properties used are determined from the following dimensionless groups:

- Reynolds number: $Re = 10,000$, based on pipe diameter, D
- Reduced Froude number: $F \equiv \frac{U}{\sqrt{g\frac{\delta\rho}{\rho}D}} = 0.67 \pm 40\%$
- Peclet number: $Pe \equiv \frac{UD}{\alpha} = 6 \times 10^4$

where U, g, ρ and α are the bulk velocity, gravitational acceleration, fluid density, and thermal diffusivity respectively.

The flow is fully developed at the inlet, and is allowed to reach a (statistically) steady isothermal state before commencing the thermal transient. A hot shock is introduced at the inlet at time t_0, and increases linearly until time t_1 where it remains at the maximum temperature. The duration of the ramp is $t_1 = t_0 + 7.5U/D$.

The ratio of thermal diffusivities is based on water flowing within a steel pipe. I.e. $\frac{\alpha_{solid}}{\alpha_{fluid}} = 144.8$.

2.2 Geometry

As shown in Fig. 2.1, the length of both vertical sections is $10D$, while the radius of curvature of both elbows is $1.5D$. The near-horizontal section is $6D$ in length, with a slope of 1%. The wall thickness is $0.05D$. For further details of the geometry, refer to [33].

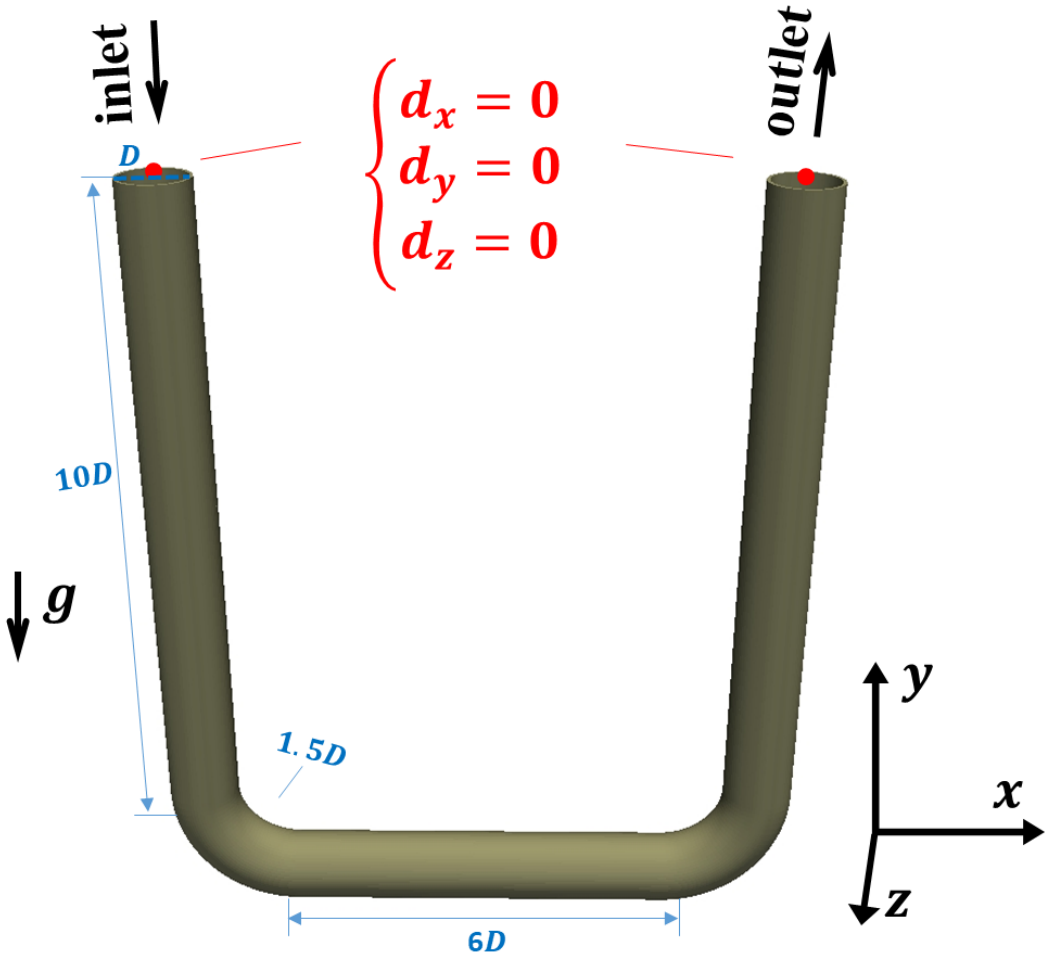

Figure 2.1: Boundary condition employed in stress analysis calculations.

2.3 Simulation setup

Conjugate heat transfer (CHT) simulations were preformed with Code_Saturne version 5.0 [9]. The coupling between solid and fluid domains was accounted for internally. A series of 22 large eddy simulations (LES) were performed, and ensemble averaged in order to generate a benchmark from which to validate the RANS results. For the LES calculations, the inflow first- and second-order statistics were generated from a pre-cursor RANS (EBRSM model [23]), and fluctuations with these statistics were generated at the inlet via the Synthetic Eddy Method [17]. Care was taken to ensure the fluctuations reached a developed state prior to the upstream bend. For the LES calculations, the fluid domain was meshed with approximately $45M$ cells, while an additional $\sim 5M$ cells were used to discretise the solid domain. In all cases, the non-dimensional cell sizes were sufficient to resolve the thermal boundary layer ($\Delta T^+ \approx 1$, $y^+ < 1$ at the wall).

Buoyancy is accounted for via a Boussinesq approximation in both the gravity source term, and the turbulence production (see Viollet [33]).

For the RANS calculations, closure of the RANS was achieved through the use of the EBRSM model. In this case, meshes comprising approximately $4M$ and $0.5M$ cells were employed for the fluid and solid domains, respectively. Mesh sensitivity tests were carried out with $1M$ and $0.1M$ cells for the fluid and solid domains, respectively (see Section 2.4 for further details).

In addition to the CHT simulations, stress analysis of the wall has been performed with FEniCS (a project for Finite Element open-source software) [2]. The displacement and stress of the pipe-wall at four time instants has been calculated. The temperature distribution of the bend at each time instant was prescribed in FEniCS. The stress calculation employed $\sim 0.5M$ tetrahedron cells for the solid domain. Linear thermo-elastic formulations were implemented within the FEniCS solver. Based on the virtual work principle, the continuum mechanics variational formulation is to find $\boldsymbol{d} \in \mathcal{D}$ such that

$$\int_\Omega \langle \boldsymbol{\sigma}(\boldsymbol{d}, T), \boldsymbol{\varepsilon}(\delta \boldsymbol{d}) \rangle \, d\Omega = \int_\Omega \delta \boldsymbol{d} \cdot \boldsymbol{b} \, d\Omega + \int_\Gamma \delta \boldsymbol{d} \cdot \widehat{\boldsymbol{tr}} \, d\Gamma \qquad \forall \delta \boldsymbol{d} \in \mathcal{D} \tag{2.1}$$

where $\boldsymbol{d}$ is the displacement vector, T is the temperature distribution, $\mathcal{D}$ denotes the displacement admissible function space, Ω is the physical domain, Γ is the boundary of the domain, b is the applied mechanical volume load and $\widehat{\boldsymbol{tr}}$ is the prescribed tractions on the Neumann boundary. The stress tensor σ is calculated as follows:

$$\boldsymbol{\sigma}(\boldsymbol{d}, T) = \langle \boldsymbol{C}, (\boldsymbol{\varepsilon} - \boldsymbol{\varepsilon_t}) \rangle = \lambda tr(\boldsymbol{\varepsilon}) \boldsymbol{I} + 2\mu \boldsymbol{\varepsilon} - \boldsymbol{\varepsilon_t} \tag{2.2}$$

where $\boldsymbol{C}$ is the constitutive tensor and $\boldsymbol{I}$ is the identity matrix. λ and μ are Laḿe coefficients. $\boldsymbol{\varepsilon}$ is the strain tensor that calculated as

$$\boldsymbol{\varepsilon} = \frac{1}{2}(\bigtriangledown \boldsymbol{d} + (\bigtriangledown \boldsymbol{d})^T) \qquad \text{in } \Omega \tag{2.3}$$

and the $\boldsymbol{\varepsilon_t}$ is the thermal strain tensor that calculated as

$$\boldsymbol{\varepsilon_t} = \alpha(3\lambda + 2\mu)(T - T_0)\boldsymbol{I} \qquad \text{in } \Omega \tag{2.4}$$

In the present case, there isn't any applied mechanical volume load or prescribed tractions. The stress-free reference temperature T_0 is set to be constant throughout the pipe. With the equations above, the thermally induced displacement and stress could be obtained. Point-based displacement constraints at both inlet and outlet of the pipe-wall have been implemented as shown in Fig. 2.1. These two constraints prevent the left and right vertical sections from diverging from one another, but allow the solid structure to expand in response to the temperature distribution.

2.4 Model Verification & Validation

2.4.1 CFD+CHT model

Mesh sensitivity

For RANS, two mesh densities have been considered. Figure 2.2 shows the coarse (1M fluid cells) and fine (4M fluid cells) give broadly similar results. A qualitative comparison is made in Figure 2.3. It can be seen that the agreement is reasonable, and the fine solution can be considered mesh independent (to within a tolerance of a few per cent). All subsequent calculations presented herein are performed with the fine mesh.

As an aside, we note challenges can arise when using probes or contour plots to assess grid convergence, particularly if probes happen to be located in regions where the temperature gradient is high. To alleviate this, we have made some preliminary developments in image based feature detection, which can automatically identify features of interest in a simulation, and assess their similarity. By assessing mesh convergence on integrated quantities, such as the area of a feature, or its centroid, similarity between features can be determined with less sensitivity to user parameters such as probe locations. In the present work, image processing has enabled the automated detection of the region of stratified flow, as seen in Figure 2.4. This prototype work could be further developed to detect features within a cognitive computing framework, thereby automating and removing bias from grid sensitivity tests. In the present study, the centroids of the red areas in Figure 2.4 matched to within a few per cent.

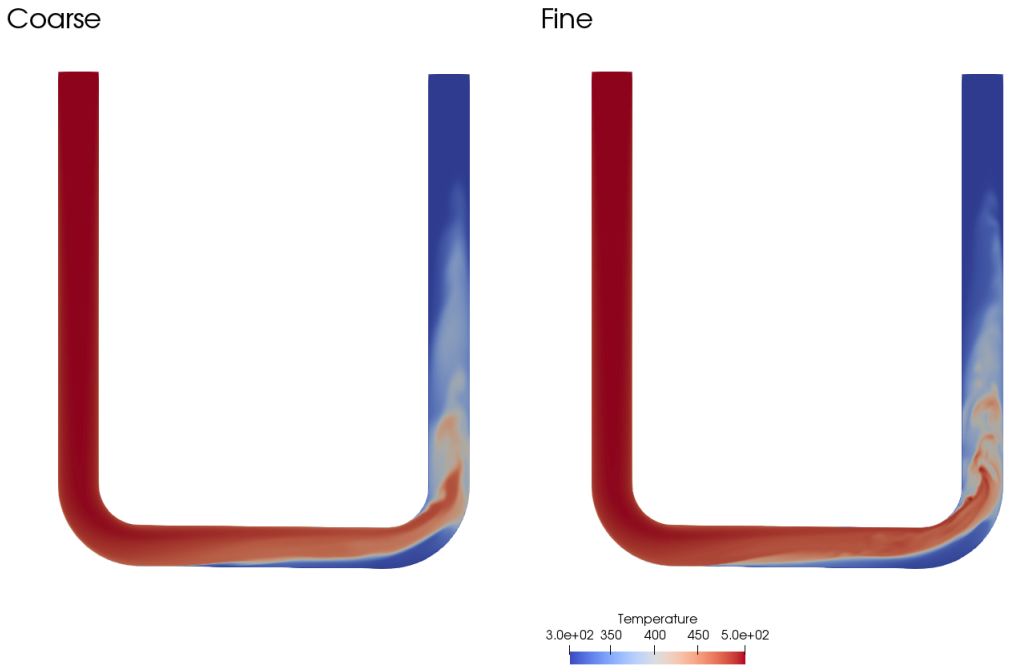

Figure 2.2: Temperature contours in the symmetry plane for coarse and fine RANS meshes at time $Ut/D = 40$. $F = 0.67$

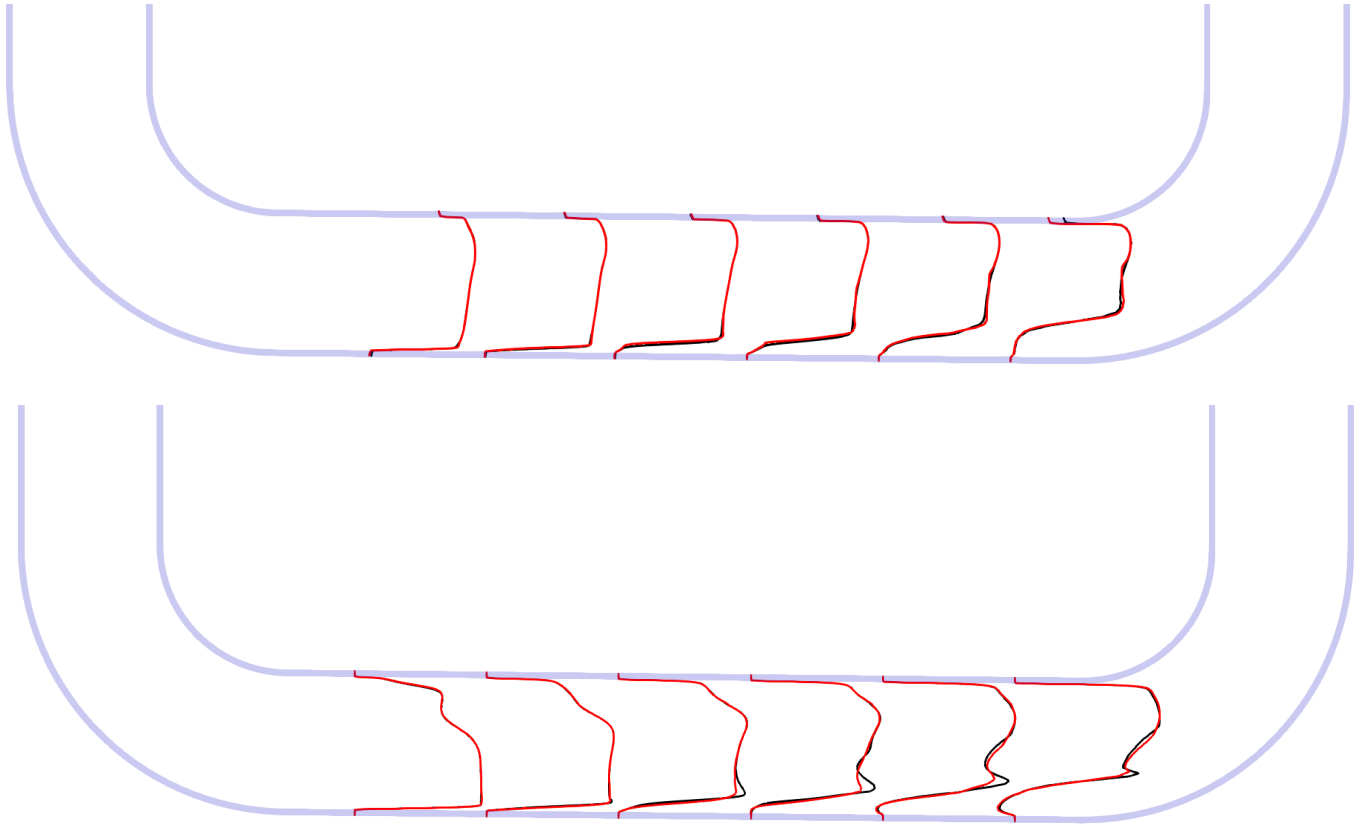

Figure 2.3: Profiles in the symmetry plane. Temperature (top) and streamwise velocity (bottom); Fine mesh (black) is compared against coarse mesh (red) at $Ut/D = 30$.

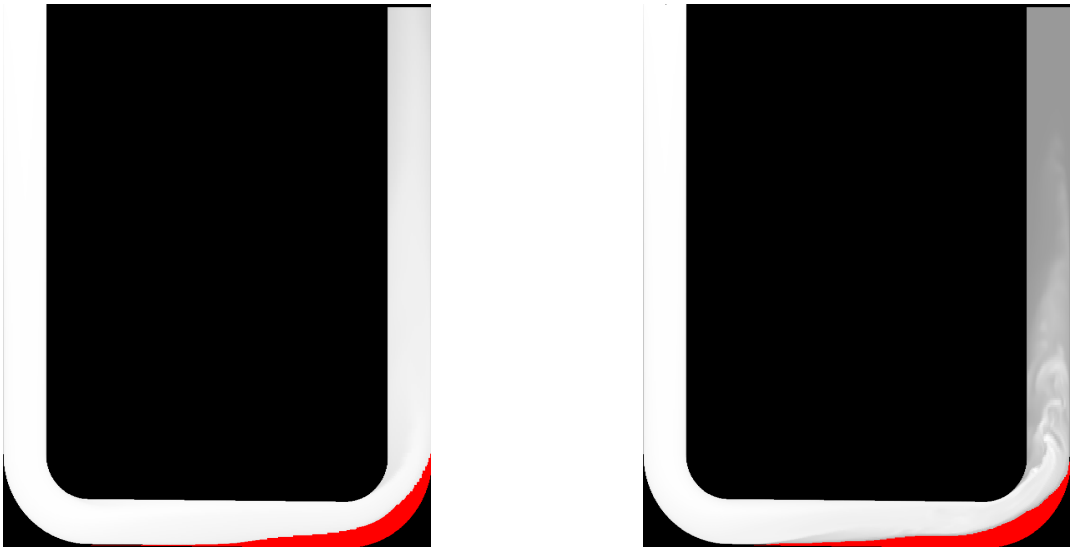

Figure 2.4: Image based automated feature recognition, showing stratified region for coarse (left) and fine (right) meshes at time $Ut/D = 40$.

Validation

Figure 2.5 shows profiles in the symmetry plane of the stably stratified region for both RANS (EBRSM) and an ensemble of LES runs. It can be seen that the temperature is predicted reasonably well by the EBRSM model, with the exception of the upper region of the wall, where the RANS tends to predict higher in-wall temperatures (presumably due to higher levels of turbulent mixing in the near-wall region).

For the velocity profiles, the agreement between RANS and LES is less satisfactory, although still broadly acceptable. The region of separated flow at the lower wall is well captured.

Comparison with higher-order statistics has not been possible, due to the large number of LES runs that would be needed to generate a reliable ensemble.

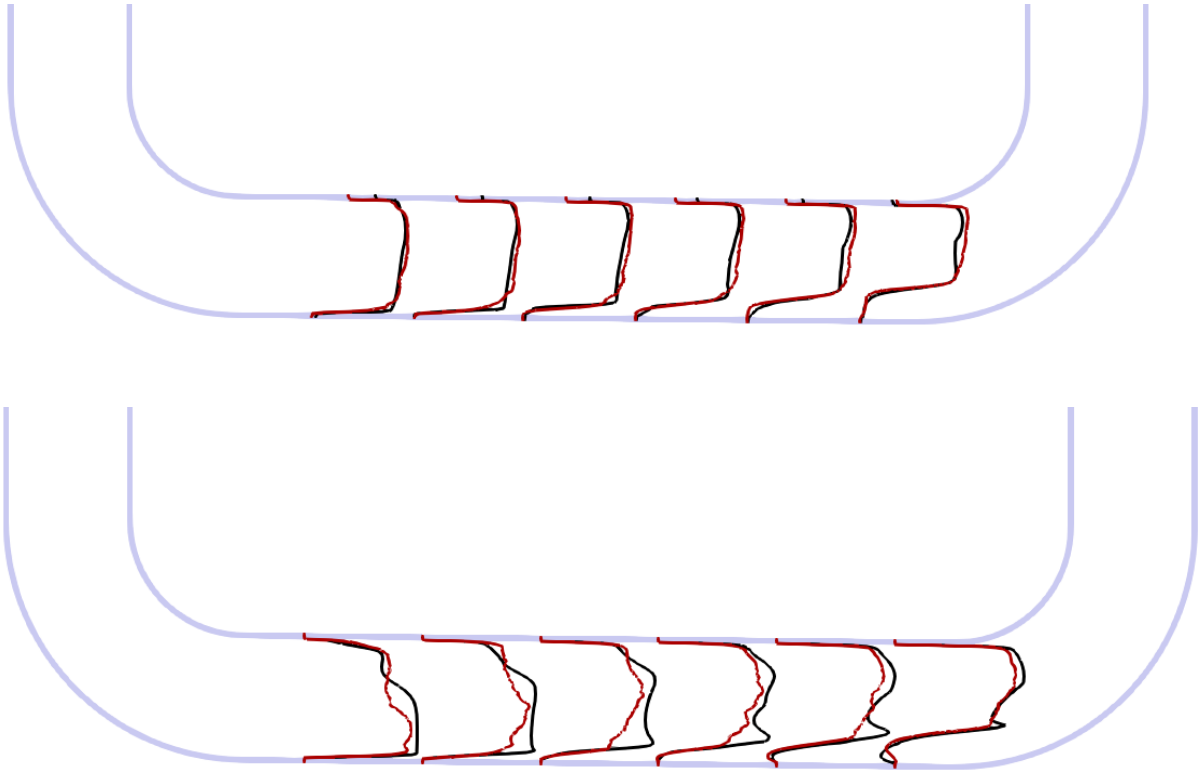

Figure 2.5: Profiles in the symmetry plane. Temperature (top) and streamwise velocity (bottom); EBRSM model (black) is compared against an ensemble of 22 LES runs (red) at $Ut/D = 30$.

2.4.2 Stress analysis model

The displacement and stress analysis of the pipe-wall is ongoing work. This section will present some preliminary results that have been obtained so far.

Displacement at different time instants

Four time instants have been considered in the calculation, which are $\tilde{t} = Ut/D = 15, 30, 45$ and 60.

Fig. 2.6 and Fig. 2.7 shows the non-dimensional displacement magnitude $|\boldsymbol{d}|/D$ contour and corresponding line plot at the non-dimensional z-axis coordinate $z/D = 0$. The two lines in the line plots represent the inner and outer intersections between the pipe-wall and the $z/D = 0$ plane. It can be seen that the maximum thermal-induced displacement of the solid wall increases with increasing wall temperature. The maximum displacement is located on the left elbow at all times. At $\tilde{t} = 60$, the maximum displacement magnitude $|\boldsymbol{d}|/D = -0.072$ at $x/D = -0.12$.

Displacement Vector

Fig. 2.8 shows the contour plot of non-dimensional displacement magnitude $|\boldsymbol{d}|/D$ and all three components of non-dimensional displacement at $\tilde{t} = 60$. Corresponding temperature distribution of the pipe-wall at $\tilde{t} = 60$ has also shown in Fig. 2.8 (e) for reference.

As can be seen from Fig. 2.8 (b), the left vertical section is displaced in the negative direction, while the right pipe has a positive displacement. A similar situation occurs for the y-axis and z-axis displacements; the pipe-wall is expanding in all three directions under the present working conditions.

Stress Tensor

Having the displacement and temperature distribution, the stress tensor of the solid wall could be obtained. The principle stress tensor components, i.e. σ_{xx}, σ_{yy} and σ_{zz}, at $\tilde{t} = 60$ are shown in Fig. 2.9. Based on these contour plots, σ_{xx} plays a dominant role among the different components of the stress tensor. There is a high σ_{xx} stress region at the bottom of the horizontal part of the pipe-wall. This is dominated by thermal expansion. The thermal stratification plays a fairly insignificant role, which is somewhat surprisingly as is different from the intuitive judgement.

The von Mises stress criteria for yielding

For ductile materials, the stress is not proportional to strain when yielding occurs. When a certain level of stress is reached the material will suffer from irreversible

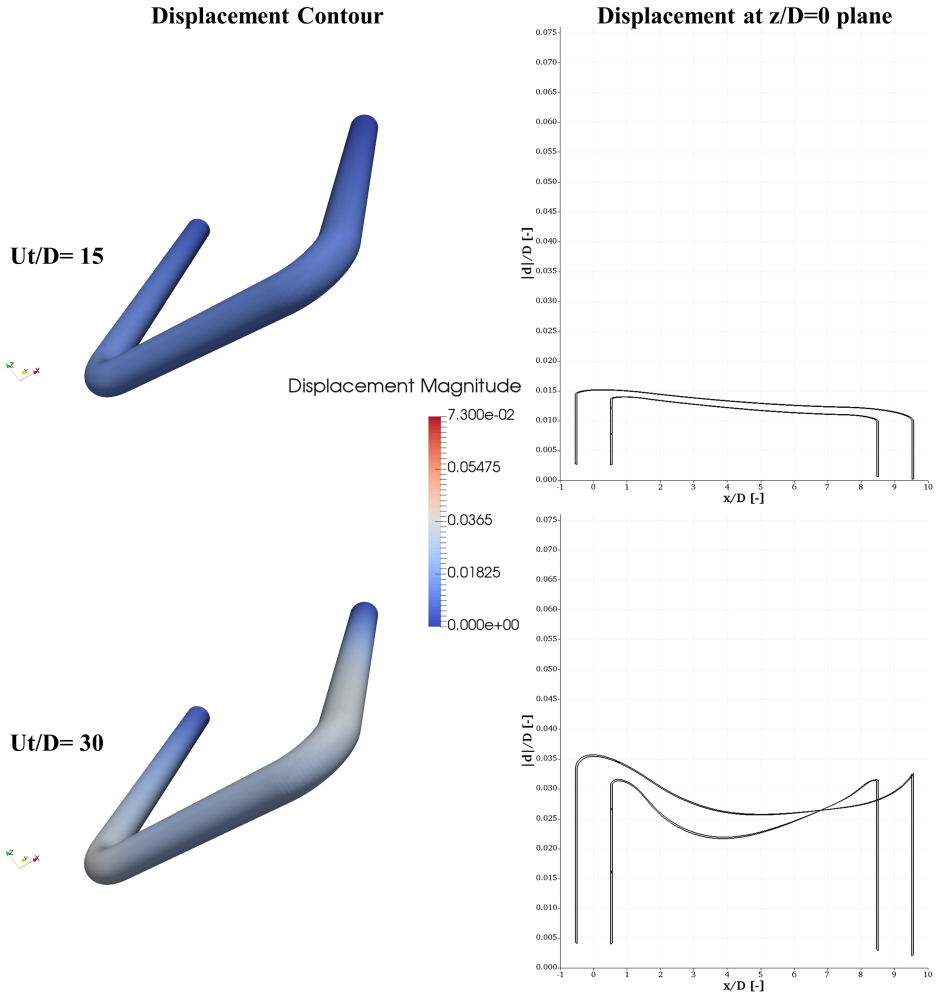

Figure 2.6: Non-dimensional displacement contour and corresponding line plots for each time instants.

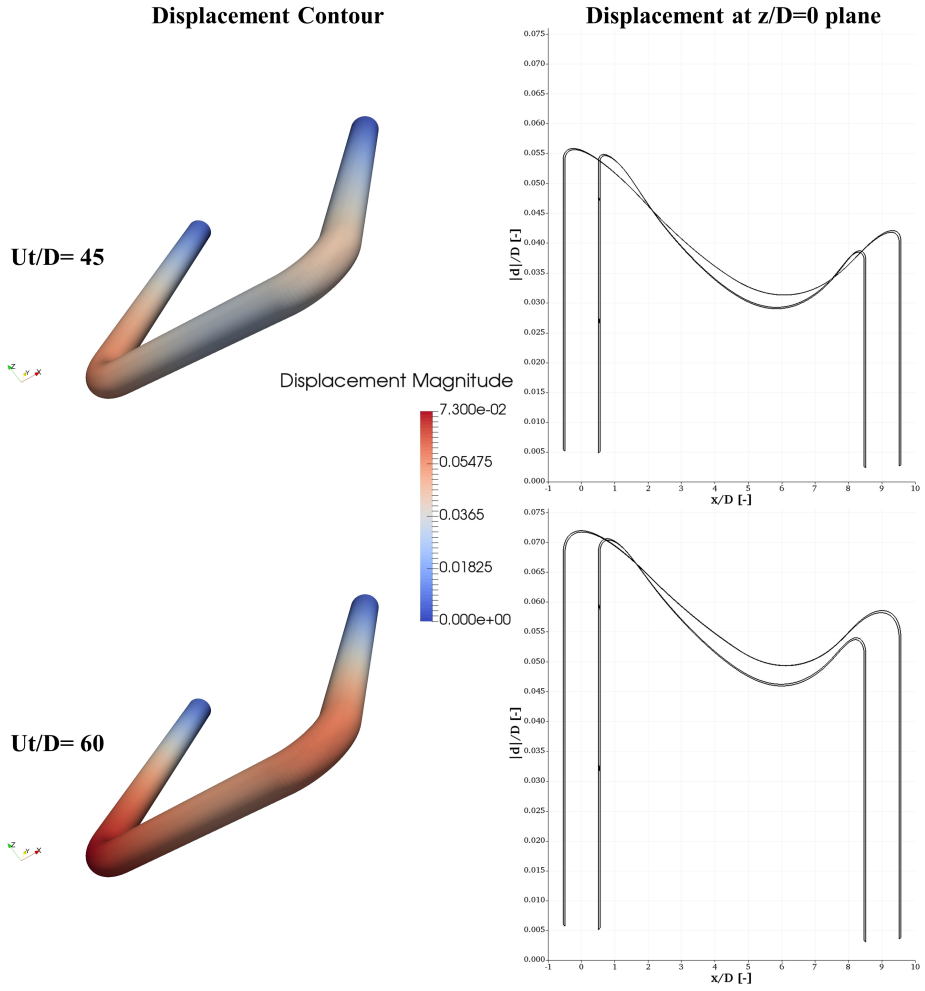

Figure 2.7: (Cont.) Non-dimensional displacement contour and corresponding line plots for each time instants.

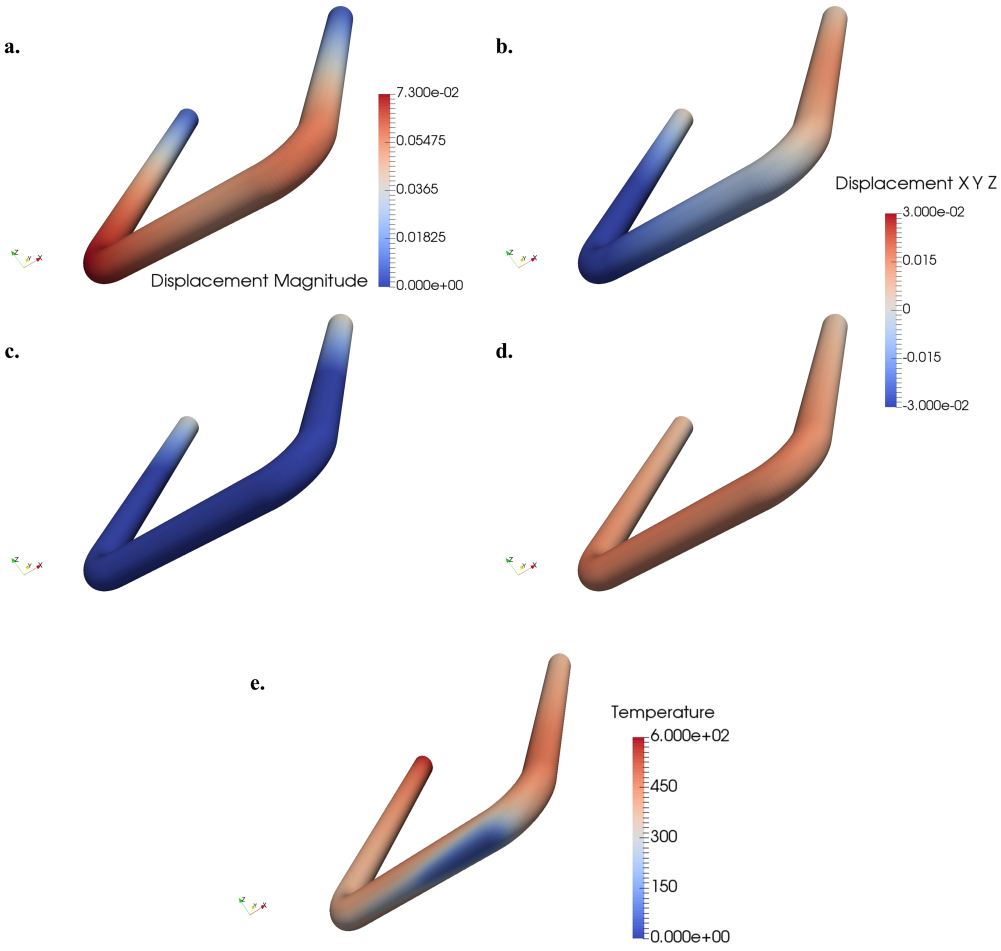

Figure 2.8: Displacement magnitude, vector components and temperature distribution contours at $\tilde{t} = 60$.

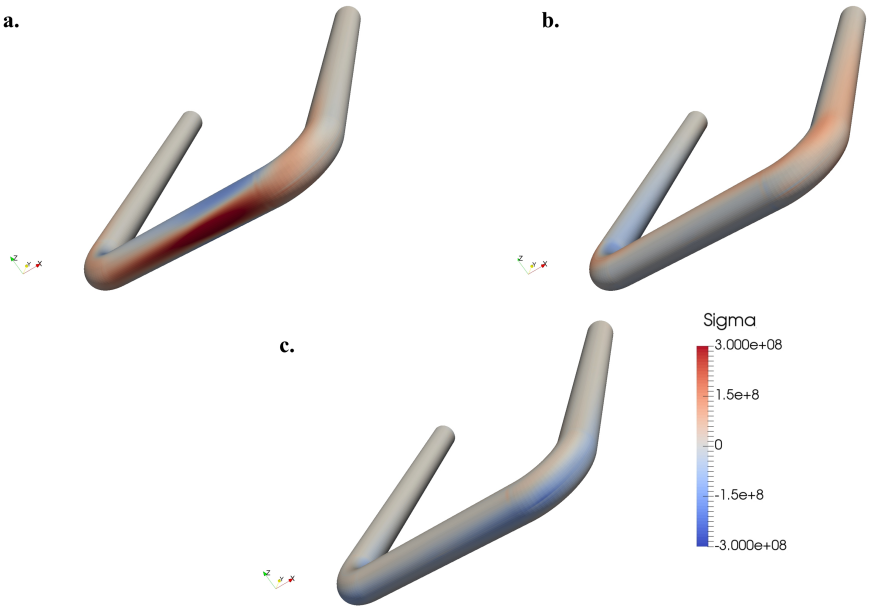

Figure 2.9: Principle stress tensor components contour at $\tilde{t} = 60$.

deformation due to the permanent molecular rearrangement of the microstructure. The von Mises yield criterion is a criteria that is found to be suitable for most ductile materials when assessing the likelihood of structural damage. The von Mises stress criterion is defined as:

$$\sqrt{\frac{1}{2}[(\sigma_{xx}-\sigma_{yy})^2+(\sigma_{yy}-\sigma_{zz})^2+(\sigma_{zz}-\sigma_{xx})^2]+3(\sigma_{xy}^2+\sigma_{yz}^2+\sigma_{zx}^2)} < \sigma_Y \qquad (2.5)$$

where σ_Y is the yield stress of the material. According to this criterion, the yielding will not occur as long as the von Mises stress (LHS of Eq. 2.5) of the solid wall is smaller than the yield stress of steel.

Fig. 2.10 shows the von Mises stress distribution. It shows a high stress region at the bottom of the horizontal part of the pipe-wall (primarily contributed by σ_{xx}). The region of von Mises stress larger than 2×10^8 Pa extends from $x/D = 1.36$ to $x/D = 8.57$.

The von Mises stress distribution along the x-axis direction at $z/D = 0$ plane is shown in Fig. 2.11. It shows that the von Mises stress keeps rising in the x-axis direction from the inlet boundary until reaches to the peak stress at $x/D = 5.28$. The von Mises stress starts to drop in the x-direction from that point to the outlet boundary.

Fig. 2.12 shows the radial von Mises stress distribution at $x/D = 5.28$ plane, i.e. the maximum von Mises stress location. It is clear that the von Mises stress is

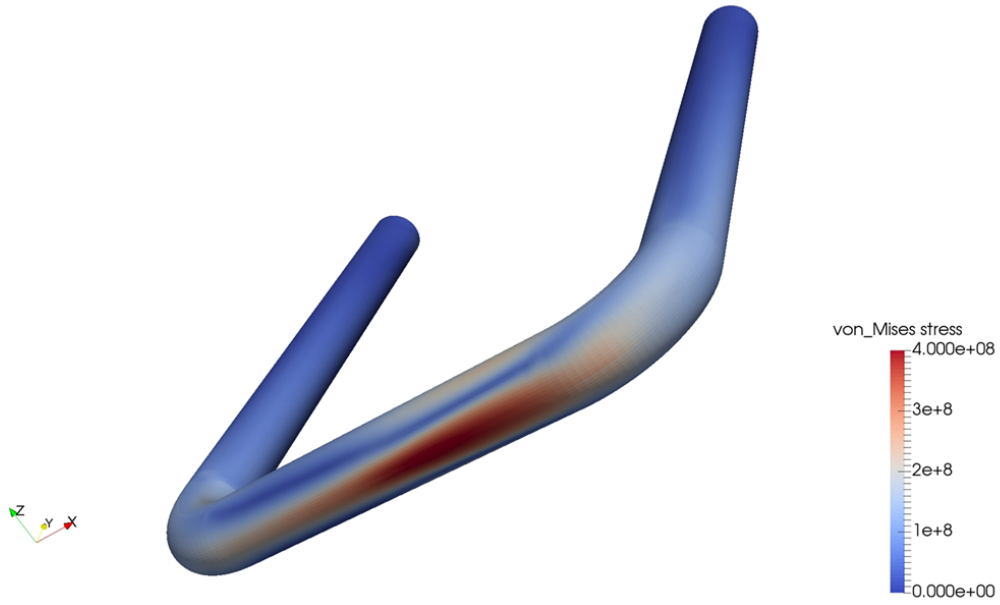

Figure 2.10: von Mises stress contour at $\tilde{t} = 60$.

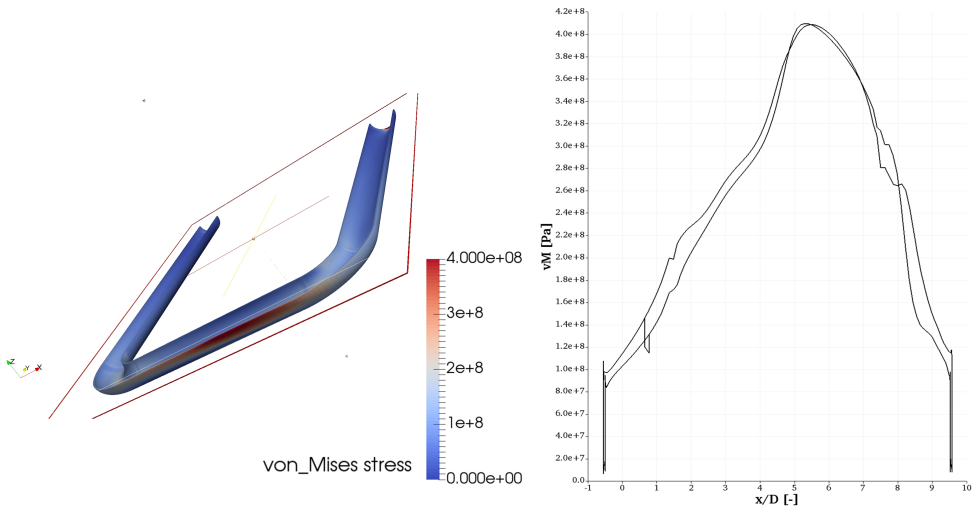

Figure 2.11: von Mises stress distribution at $z/D = 0$ plane at $\tilde{t} = 60$.

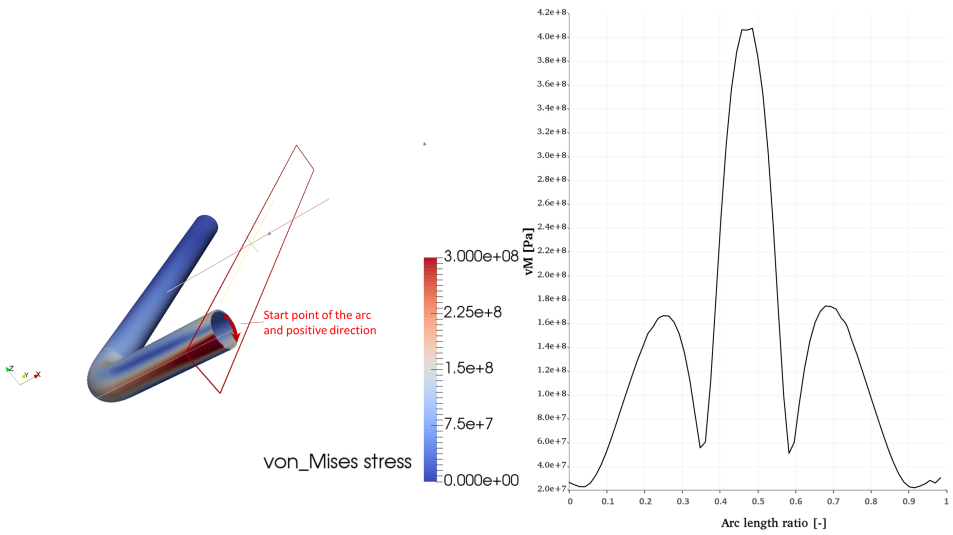

Figure 2.12: Radial von Mises stress distribution at $x/D = 5.279$ plane at $\tilde{t} = 60$.

symmetrically distributed about the $z/D = 0$ plane and the maximum von Mises stress is located at the $z/D = 0$ and at the arc length of 0.5.

The maximum von Mises stress of the present case is 4.09×10^8Pa. With a 30% margin of safety, the yield stress of the material would be around 5.32×10^8Pa, as to prevent yielding and failure of the solid wall.

Table 2.1 summarizes the yield stress of some common types of steel. It can be seen that the stress caused by the thermal transient at the present working condition beyond the yield criteria of ASTM A36, while approaching the yield criteria of API 5L X65 and high strength alloy ASTM A514. According to the fatigue theory, the fatigue life of the pipe-wall and the magnitude of stress are negatively correlated.

Table 2.1: Yield stress of comment types of steel.[1, 15]

Steel Type	**Yield stress [Pa]**
Steel, ASTM A36	2.50×10^8
Steel, API 5L X65	4.48×10^8
Steel, high strength alloy ASTM A514	6.90×10^8
Steel, pre-stressing strands	1.65×10^9

Chapter 3

Uncertainty quantification - theory

There are two common categories of discrepancies identified both in physical and numerical experiments: *aleatoric* and *epistemic*. The first type refers to uncertainty due to the physical variability of a system (irreducible), while the latter arises from a lack of knowledge (reducible). UQ in computer experiments comprises rigorous analysis of the epistemic errors. These can further be classified as uncertainties related to model inaccuracy and parametric uncertainties caused by imprecise values of the input coefficients.

Of particular interest in modelling of real-world problems is parametric UQ, which is identified as a crucial component of simulation-based reliability analysis. To increase confidence and the utility of modelling predictions, we need to account for discrepancies which stem naturally from our limitations in measuring and manufacturing.

Conventional non-intrusive approaches for UQ are based around Monte Carlo (MC) analysis which requires a large number of simulations for different sets of input parameters. An alternative strategy uses a smaller number of realisations to build a surrogate model which approximates the response of the original simulator. Common surrogate-based methods are polynomial chaos (PC) and Gaussian process emulation [31].

3.1 Generalised polynomial chaos

We are considering the Foude number $Fr(\xi)$ to be a random variable, where ξ has a certain probability measure μ on $\Omega \subseteq \mathbb{R}$. We want to measure the effect on the temperature distribution along the pipe. More detailed description of the problem is provided in Sec. 2. In this report, the real-valued random variable is represented by $Y(\xi)$.

Given the uncertain input, the CFD prediction of quantity of interest (QoI) can

be represented as a PC expansion as follows:

$$Y(\xi) = \sum_{k=0}^{\infty} y_k \psi_k(\xi), \tag{3.1}$$

where the basis functions ψ_k are orthogonal with respect to measure μ and $\{y_k\}_{k=0}^{\infty}$ is a set of PC coefficients. The study can be extended to the $\mathbb{R}^n$-valued random variable, $\mathbf{Y} = \{Y_1, \ldots, Y_n\}$, where

$$\mathbf{Y}(\xi) = \sum_{k=0}^{\infty} \mathbf{y}_k \psi_k(\xi), \tag{3.2}$$

with $\mathbf{y}_k = \{y_{1,k}, \ldots, y_{n,k}\} \in \mathbb{R}^n$ for each $k \in \mathbb{N}_0$; dependence of QoI on multiple sources of uncertainty $\boldsymbol{\xi} = \{\xi_1, \ldots, \xi_\alpha\}$, can also be considered. In practice, the series expansion is truncated after $P + 1 = (\alpha + p)!/\alpha!p!$ terms, where α defines the stochastic dimensionality and p is the order of the corresponding multivariate polynomials, $\Psi_k(\boldsymbol{\xi})$. Such representation (including the truncated series) allows for straightforward stochastic post-processing; the measurement of the expected value of Y is simply its zeroth PC coefficient, $\mathbb{E}[Y] \langle \Psi_0 Y \rangle = \sum_{k=0}^{P} y_k \langle \Psi_0 \Psi_k \rangle = y_0$, while the variance is defined as

$$\mathbb{V}[Y] = \mathbb{E}\left[|Y - \mathbb{E}[Y]|^2\right] = \sum_{k=0}^{P} y_k^2 \left\langle \Psi_k^2 \right\rangle. \tag{3.3}$$

As the total number of PC coefficients grows combinatorially (*curse of dimensionality*) as a function of the number of random inputs and polynomial order, p, practical applications of the expansion are limited to studies with low stochastic dimension [31].

Wiener [36] introduced PC expansions, where Hermite polynomials were used to model stochastic processes with Gaussian random variables. The extension to generalised PC developed by Xiu [39] allows for non-Gaussian random processes. In the generalised polynomial chaos approach, different orthogonal polynomials in the Askey scheme are incorporated for different distribution types. In this report, the abbreviation PC refers to a generalised formalism of Wiener's approach.

Considering its practical implementation, there are two main strategies for determining the expansion coefficients, y_k, in Equation (3.1). The PC expression of random variables can be directly introduced to the model equations, and a Galerkin projection is then applied to obtain a stochastic solver [38, 31]; hence, the approach is referred to as the *intrusive spectral projection* (ISP). Xiu [38] explains that although the Galerkin formalism offers the most accurate solutions, it is not suitable for highly complex models. It is also not recommended when the UQ analysis is performed on *legacy codes*, which are often not amenable to changes. The opposite situation is for non-intrusive methods which rely on individual realisations of

Y to determine the response of the system to random inputs. In this approach, the deterministic solution does not need to be modified and can be evaluated at any desired point of the probability space $(\Omega, \mathcal{F}, \mu)$. Here Ω defines a sample space which contains all possible outcomes, while $\mathcal{F}$ is a σ-algebra (a set of events), and μ is the probability measure which defines event's likelihood. If the normalisation constant, $\gamma_k = \langle \Psi_k^2 \rangle$, is known, in non-intrusive spectral projection (NISP), the PC coefficients

$$y_k = \frac{\langle Y \Psi_k \rangle}{\langle \Psi_k^2 \rangle} = \frac{1}{\gamma_k} \int Y(\xi) \Psi_k(\xi) d\mu(\xi), \quad k = 0, \ldots, P \tag{3.4}$$

can be obtained by approximating the integral with *quadrature rules*. The realisations of Y are used to determine a surrogate model $\tilde{Y}$ for which

$$\tilde{Y} = \sum_{k=0}^{P} \tilde{y}_k \Psi_k \approx Y, \tag{3.5}$$

where $\tilde{y}_k = \frac{1}{\gamma_k} \sum_{j=1}^{Q} y\left(\xi^{(j)}\right) \Psi_k\left(\xi^{(j)}\right) w^{(j)}$ and $\left(\xi^{(j)}, w^{(j)}\right)$ are the prescribed nodes and their corresponding weights. Sullivan [31] states that if the dimensionality of vector $\boldsymbol{\xi}$ is small and $Y(\boldsymbol{\xi})$ is relatively smooth, the Gaussian quadrature approximation (nodes at the roots of μ-orthogonal polynomials) is an optimal choice. This quadrature yields an exact result for polynomials of degree at most $2Q-1$, where Q is the number of quadrature nodes. For multi-dimensional stochastic domains, sparse quadrature rules may be used to partially alleviate the curse of dimensionality.

Another non-intrusive approach to estimate the expansion coefficients, y_k is regression, which uses the least-squares solution to a linear system [26]. For the regression, the expansion coefficients are found by minimising the sum of the squared difference between observed data $\mathbf{Y} = [Y_1, \ldots, Y_M]$, where $Y_m = Y\left(\xi^{(m)}\right)$ for $m = 1, \ldots, M$, and the truncated PC expansion, $\tilde{Y} = \sum_{k=0}^{P} \tilde{y}_k \Psi_k$ with $\tilde{\mathbf{y}}_k = (\tilde{y}_0, \ldots, \tilde{y}_k)$

$$\tilde{\mathbf{y}}_k = \arg \min_{\mathbf{y} \in \mathbb{R}^{P+1}} \left[\sum_{m=1}^{M} \left(Y\left(\xi^{(m)}\right) - \tilde{Y}\left(\xi^{(m)}\right) \right)^2 \right]. \tag{3.6}$$

The least-squares solution is

$$\tilde{\mathbf{y}}_k = \left(A^T A\right)^{-1} A^T \mathbf{Y}, \tag{3.7}$$

where A is a data matrix containing $P+1$ multivariate polynomial terms, evaluated at the M design points

$$A_{mk} = \Psi_k\left(\xi^{(m)}\right), \quad m = 1, \ldots, M, \quad k = 1, \ldots, P+1. \tag{3.8}$$

This approach is also known as point-collocation. To have a well-posed problem, the design size, M, should be greater than or equal to the number of expansion terms $P + 1$.

In this work, the NISP is performed with the newly developed application QUTE (Quantification of Uncertainty Toolkit for Engineering), described in Appendix A. In addition, the results obtained with quadrature rules are compared with classical Monte Carlo and least-squares approximation. More information about other UQ methods is given in Appendix B.

Chapter 4

Stochastic heat transfer modelling

In this section, the methodology used for stochastic modelling of thermal stratification is discussed.

4.1 UQ procedure

We consider a one-dimensional stochastic study. The value of dimensionless Froude number has been assigned a uniform probability distribution, $h(\xi) \sim \mathcal{U}(Fr_{\min}, Fr_{\max})$, where $Fr_{\min} = 0.402$ and $Fr_{\max} = 0.938$ resulting in different mixing properties and formation of stratification layer.

The sample points in probability space, for which the CFD model is evaluated, are specified through $(p+1)$-order Gaussian quadrature selected for the given distribution. Gaussian-type quadrature rules are standard choice for polynomial chaos [31] as they account for the probability weight in the integral in Eq. 3.4.

Having determined nodes, $Fr_1, \ldots, Fr_{p+1}$, and corresponding weights, we perform the RANS simulations and use the temperature evaluations to describe the stochastic response to the uncertain parameter. Polynomials of order p are computed using a three-term recurrence relation [10]. We then use the basis, quadrature nodes, weights, and model samples to create the surrogate model, $\tilde{Y}_T$.

The surrogate model, $\tilde{Y}_T$, is used to construct a response probability density function (PDF). The cost of the procedure is very low in comparison with evaluating the PDF with the original model, Y_T, which requires a full CFD simulation.

In general, there is no special rule for selecting the values of the maximum PC expansion order – the choice is also problem-dependent. Therefore, the usual approach is to start with a small value and, by increasing the order of the expansion, the convergence of stochastic moments can be monitored. This procedure can be repeated until the desired accuracy is achieved.

4.2 Convergence of UQ

Having the polynomial chaos expansion, it is necessary to evaluate the accuracy of the surrogate model. In the present work, the convergence analysis of resulting statistical moments, mean and standard deviation, is performed. As the real values are unknown, the error of approximation is estimated using results from consecutive polynomial resolutions. Therefore, the convergence error of expected value E obtained with p-th polynomial order is defined as

$$\text{Error} = \frac{|E_p - E_{p-1}|}{|E_{p-1}|}, \tag{4.1}$$

where $|.|$ denotes L_2 norm.

If the regression approach is used for estimating PC coefficients, a suitable technique for error analysis could be the leave-one-out method [25], where a surrogate is constructed using all samples except one, while the remaining sample is used for assessing the model accuracy.

Chapter 5

Results of UQ analysis

This section discusses the results of applying generalised polynomial chaos approach to RANS model of thermal dynamics of hot fluid flow in u-shaped pipe. The Gaussian quadrature approximation was used for calculating polynomial coefficients. The comparison of the UQ method with the Monte Carlo approach is presented.

5.1 Numerical results

We aim to estimate the temperature distribution in a pipe as a function of the Froude number, to gain better understanding of stratified flow development. We measure the wall temperature at rings shown in Fig. 5.1. For the UQ analysis, we apply the one-dimensional PC expansion ($\alpha = 1$) with increasing polynomial order, p. The surrogate is built for the second ring at non-dimensionalised $\tilde{t} \equiv Ut/D = 40$; at this time a stable stratification occurs as shown in Fig. 5.2 The convergence of the stochastic moments - mean, E, and standard deviation, SD, are shown in Fig. 5.3a- 5.3b and Fig. 5.3c- 5.3d, respectively. As this is a one-dimensional stochastic problem, using a polynomial of order p translates to performing $p+1$ calculations with quadrature nodes as input values. The small change in accuracy suggests that polynomial order as small as $p = 10$ can suffice to obtain a surrogate model and no more calculations are necessary. This can be further demonstrated by comparison with higher order expansion. Figures 5.4a and 5.4b show the resulting mean temperature obtained with the approximation functions, for $p = 10$ and $p = 17$, over the entire random space. The surrogates were built with simulator outputs for the set of quadrature nodes (marked as red dots). The remaining points (blue markers) are additional simulation results for different Fr numbers used here for validation. We can see that the surrogates with $p = 10$ and $p = 16$ give a comparable approximation of modelled data and can lead to accurate statistics with respect to the provided PDF.

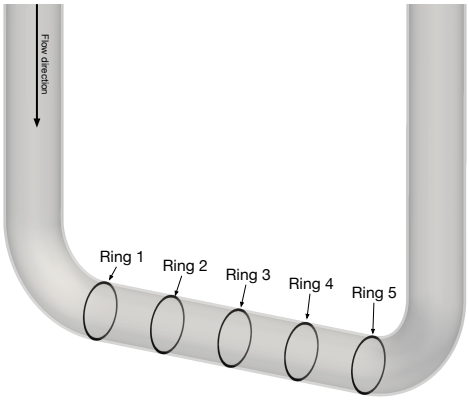

Figure 5.1: Sketch of ring locations. Rings are located at $x/D \approx 1.5, 3, 4.5, 6$ and 7.5 for rings 1 to 5 respectively, and have radius $0.525D$ (i.e. in the middle of the wall).

The resulting mean temperature distribution and standard deviation are plotted in Fig. 5.5a. Such representation of results suggests that each value of temperature within uncertainty range is equally possible to occur. However, a detailed picture in Fig. 5.5b provided by PDFs of the simulation outputs gives an interesting insight – the distribution of QoIs is bimodal in nature, i.e. extreme values of temperature are more likely to occur. This observation highlights misinterpretation of the system response in finite order statistics such as the mean and standard deviation, particularly for the under-sampled problem. The result stresses the need for performing UQ analysis. Traditional engineering approach would be to make decisions based on the mean distribution. However, in case of bimodal nature of the outputs, that would be wrong, as the expected values are not likely to be observed.

Gaussian quadrature nodes are not nested – when the polynomial order is increased to p, the nodes from the lower resolution $p-1$ cannot be re-used. If evaluations of the simulator are computationally expensive, this can be a major concern. If we do not wish to have to discard past solutions, Clenshaw–Curtis quadrature rules might be preferable. In many circumstances, they have a comparable accuracy to Gaussian quadrature [32]. Another possibility is to apply the regression approach for estimation of PC coefficients. Using the one-dimensional surrogate model built with $p = 10$ as the true estimate, we can analyse the convergence of least-squares solution to a linear system with the design size $M > p$. In Ref. [16], it is suggested to use a twice over-determined system, $M = 2 \times (p+1)$, but we also experiment with $M = p+1$ samples. The results for increasing polynomial order are plotted in Fig. 5.6 and Fig. 5.7 for the uniquely-determined and over-determined systems, respectively. The relative errors are calculated based on the true mean, E_{pc} and standard deviation, SD_{pc}, obtained in previous study with Gaussian quadratures. We analyse how quickly we can converge to the solution at

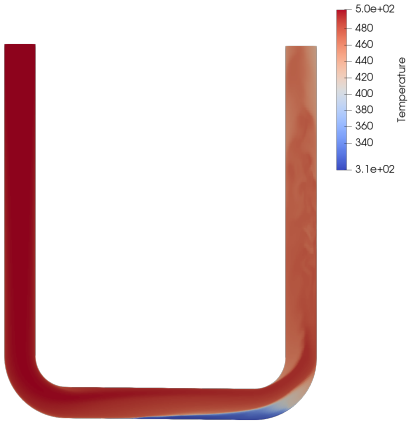

Figure 5.2: Temperature distribution in a u-shaped bend at non-dimensionalised time $\tilde{t} = 40$ for $Fr \approx 0.621$.

a given point (temperature value in the middle of the profile shown in Fig. 5.5a) using Latin hypercube sampling. We can also explore nested sampling, such as Hammersley [37]. For future work, to avoid bias, the regression study should be confirmed by using the evaluations of the CFD model to compute the surrogate.

To estimate the number of calculations necessary for obtaining the statistics with classical Monte Carlo approach, we again use the surrogate model built with PC and $p = 10$. We randomly draw samples from the uniform distribution of Fr numbers and calculate the resulting stochastic moments. Figures 5.8a- 5.8d show how slowly the method converges to the true value of mean, E_{pc}, and standard deviation, SD_{pc}, which were previously computed with only 11 simulations for PC expansion. However, the convergence of MC can in some problems be improved by applying quasi-random sampling techniques.

5.1.1 Multi-element polynomial chaos

Having performed a number of calculations, we can estimate the stochastic orthogonal approximations of temperature at any point in time and space. Figures 5.9a, 5.9c and 5.9e show temperature PDFs at rings closer to the right bend of the pipe. Corresponding surrogates are shown in Fig. 5.9b, 5.9d, 5.9f. The results are obtained with high polynomial orders, $p = 16$ or $p = 17$. However, surrogates built with smaller number of nodes allow to accurately describe stochastic moments. Expected value can converge for $p = 5$. More polynomial terms are retained due to complexity of the functions that describe input-output relationship. For the last ring, even the model with $p = 17$ does not return all of the simulation points (see Fig. 5.9f). But using polynomials of higher degree will lead to a

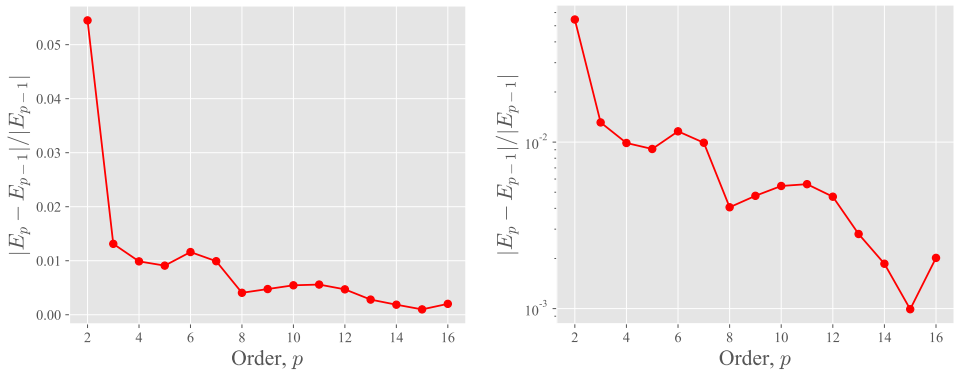

(a) Convergence of mean.

(b) Semi-log plot.

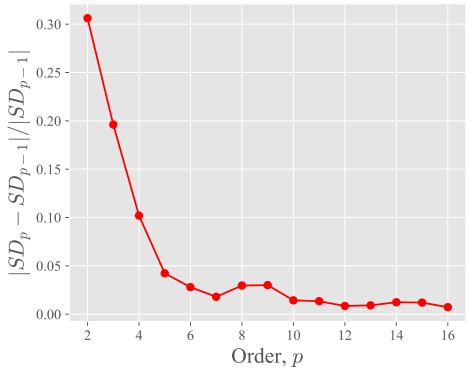

(c) Error in standard deviation.

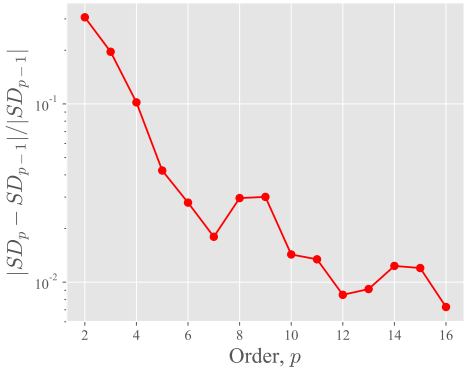

(d) Semi-log plot.

Figure 5.3: Error in expected value and standard deviation of temperature. Statistics were obtained from surrogate models built with increasing polynomial order.

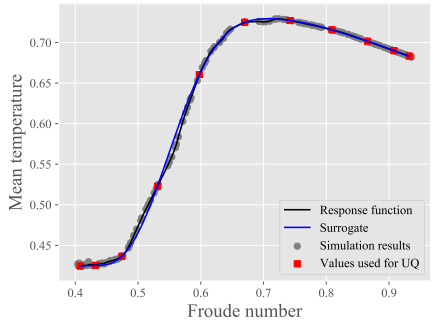

(a) $p = 10$.

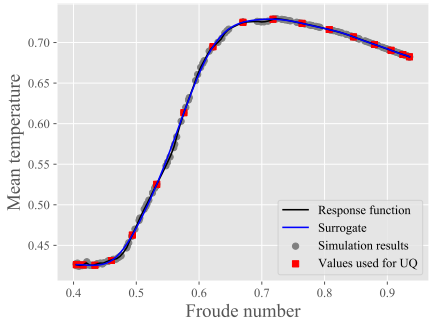

(b) $p = 16$.

Figure 5.4: Mean temperature as a function of Froude number obtained from two surrogate models – with polynomial order $p = 10$ and $p = 16$.

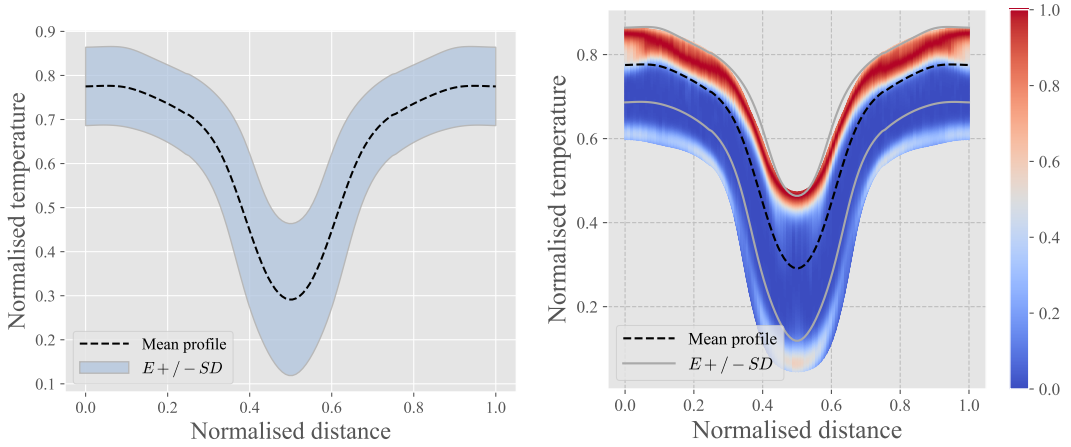

(a) Mean and standard deviation. **(b)** PDF.

Figure 5.5: Statistics derived from the PC-based surrogate with $p = 10$.

behaviour similar to *Runge phenomenon* – oscillations at the edges of an interval. Some artefacts can already be observed in Fig. 5.9d.

It is well known that although global PC can achieve exponential convergence for smooth problems, it may converge slowly or even fail in case of discontinuities or steep changes in random space [38]. This problem is observed in approximating the response of mean temperature for the first ring at $\tilde{t}$ to different Fr numbers. To circumvent this limitation, it is advised to use multi-element PC with piecewise low-degree polynomial basis [34, 11] or expansions with locally supported wavelets [20]. Figures 5.10a and 5.10b showcase the improvement in surrogate modelling when using piece-wise smooth polynomials. By adaptively dividing the random space into sections and constructing partial model response functions, we can obtain a better approximation (see Fig. 5.10b) as with global basis. The individual polynomial order of each surrogate was kept low, $p = 3$. Therefore, a better model approximation was achieved at comparable computational cost as for the global basis with $p = 17$. The mean of relative error, $\delta = \frac{1}{N}\sum_{n=1}^{N} |Y(Fr_n) - \tilde{Y}(Fr_n)|/|Y(Fr_n)|$ for the partial surrogates was $\delta = 0.0011$, while the error of the global approximant was about 5 times higher. Note, it is not required for the surrogate to go through all the simulation points (it's not an interpolation!) to accurately reconstruct the stochastic moments.

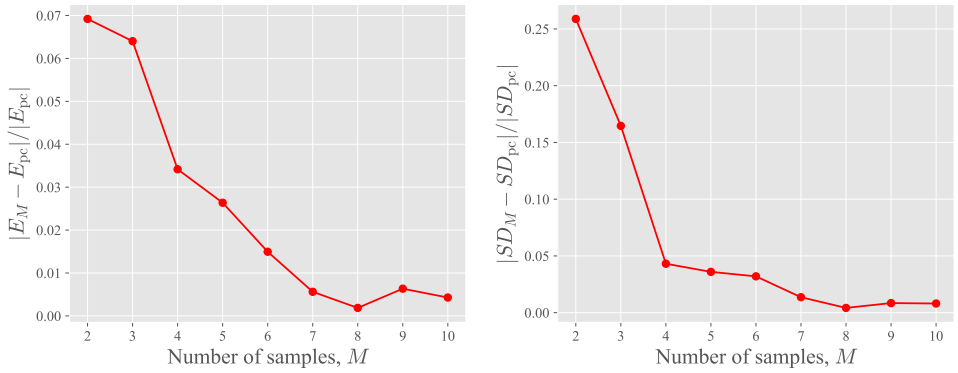

(a) Relative error of expected value. **(b)** Convergence of standard deviation.

Figure 5.6: Convergence study for one-dimensional regression-based PC with $M = p + 1$ and Latin hypercube sampling.

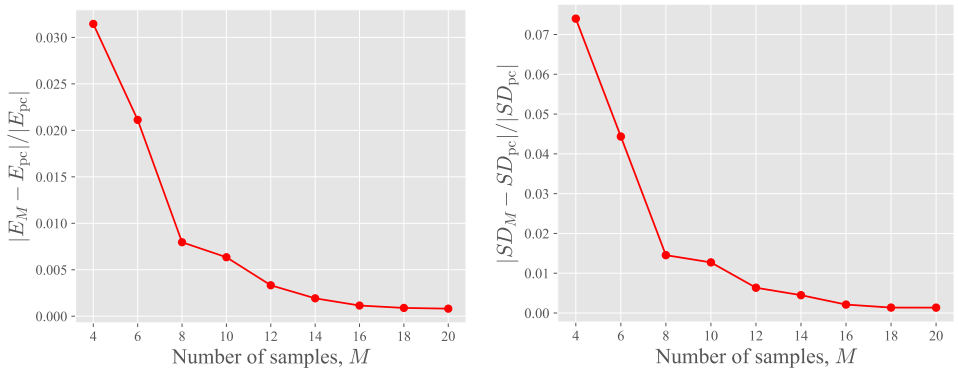

(a) Relative error of expected value. **(b)** Convergence of standard deviation.

Figure 5.7: Convergence study for one-dimensional regression-based PC with $M = 2 \times (p + 1)$ and Latin hypercube sampling.

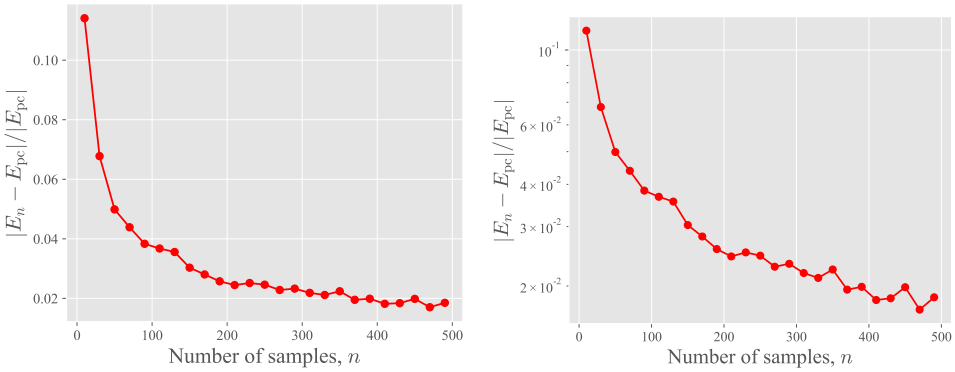

(a) Relative error of expected value.

(b) Semi-log plot.

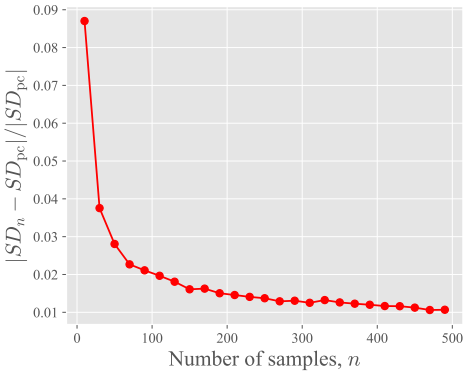

(c) Convergence of standard deviation.

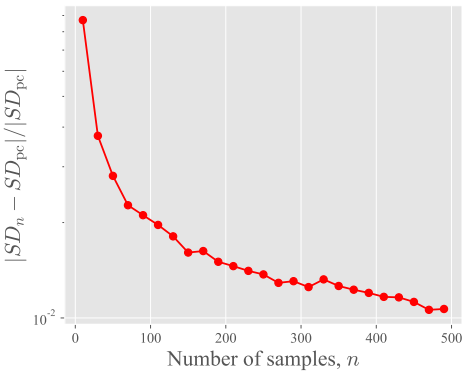

(d) Semi-log plot.

Figure 5.8: Convergence study of classical Monte Carlo for point temperature value.

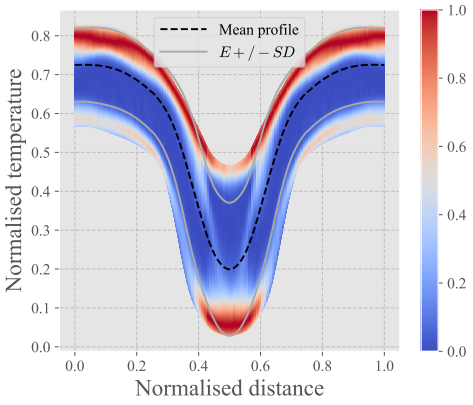

(a) PDF of 3rd ring.

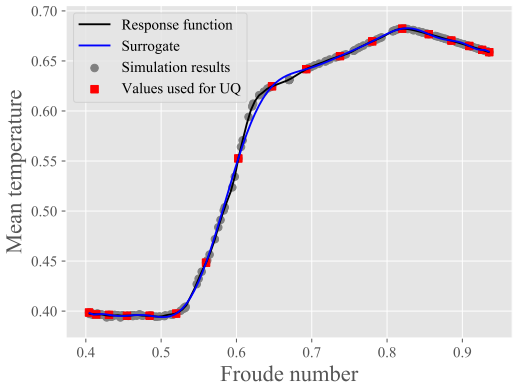

(b) Surrogate with $p = 17$.

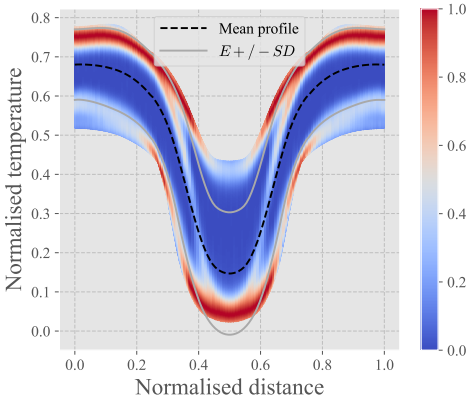

(c) PDF of 4th ring.

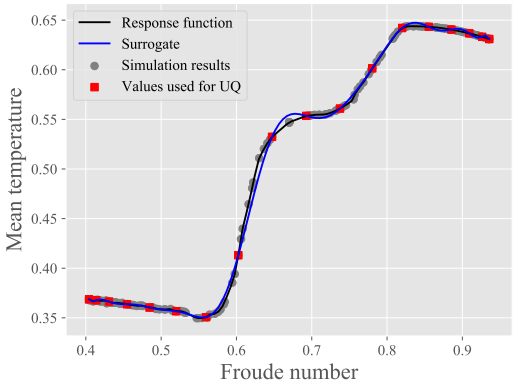

(d) Surrogate with $p = 17$.

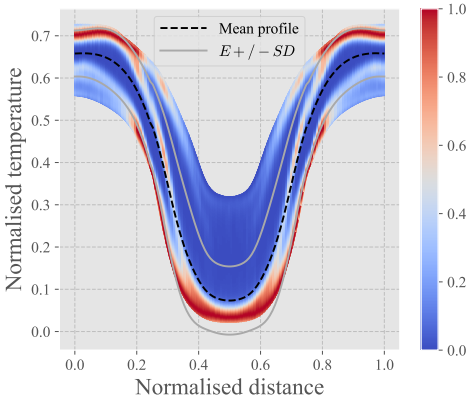

(e) PDF of 5th ring.

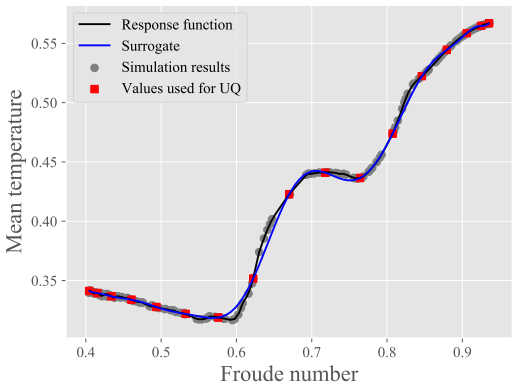

(f) Surrogate with $p = 16$.

Figure 5.9: Surrogates of temperature and the resulting PDFs at different locations in the pipe. Note, red dots are the simulator outputs for which the surrogates are generated. Blue markers are simulation results used to validate the reduced models.

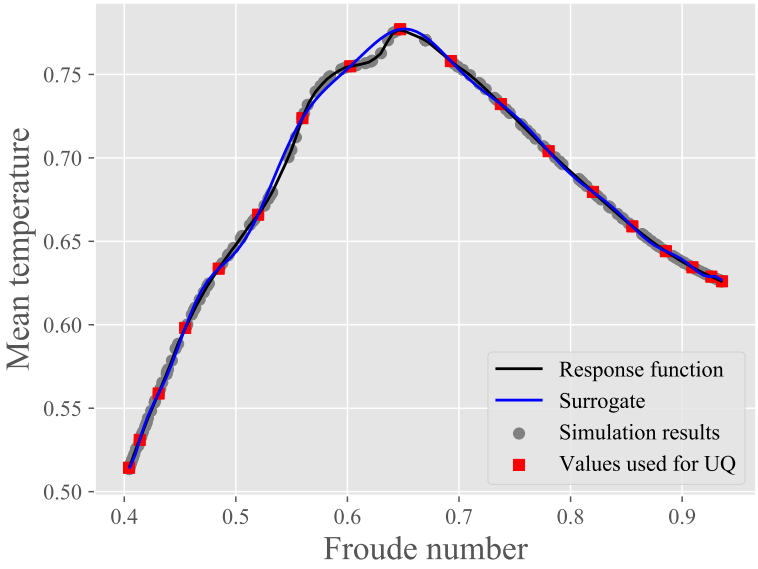

(a) Surrogate for 1st ring with $p = 17$.

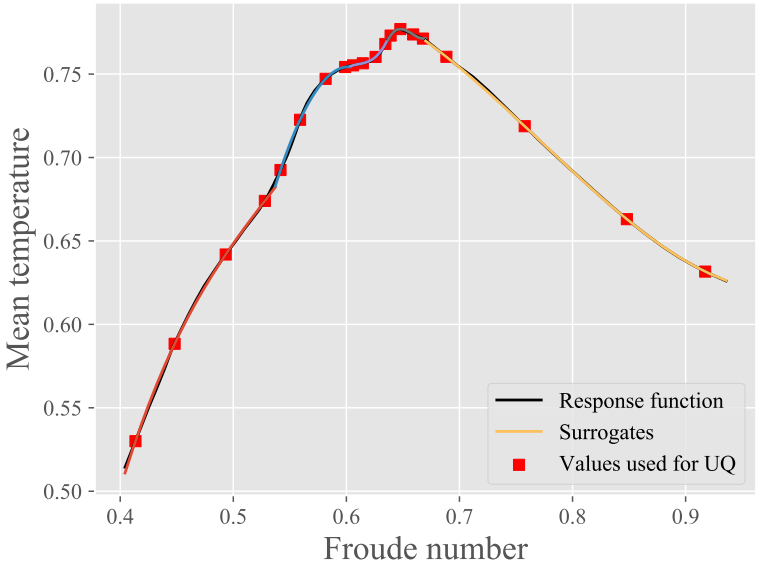

(b) Surrogate built with piece-wise smooth polynomials.

Figure 5.10: Comparison between a surrogate constructed with a global basis and a set of locally supported polynomials.

Chapter 6

Conclusions and recommendations

An ensemble of LES calculations have been conducted to provide a useful benchmark case to test RANS models. Additional RANS calculations, using the EBRSM closure, have shown reasonable agreement with the LES for this challenging case (involving stratification, transient flow, and conjugate heat transfer). Using this RANS model, we have applied a non-intrusive polynomial-based approach to model uncertainty associated with input Froude number in conjugate heat transfer modelling. The results gave an important insight – the resulting distribution of temperature is bimodal in nature. The extreme values of the variable are more likely to occur than the average profile. This observation highlights misinterpretation of the system response in finite order statistics such as the mean and standard deviation. In addition, the study of response functions shows that in this case piece-wise polynomials are better suited for constructing accurate surrogates (this is likely to be true for other stratified flow simulations).

We also showed that the knowledge extracted from the modelled system can be maximised by using surrogate-based UQ analysis, allowing the prediction of the influence of varying conditions on quantities of interest. This can be done without changing existing simulation codes, and at much smaller cost than using traditional Monte Carlo – at least an order of magnitude less calculations needed. The method is a very powerful extension of simulation which provides foundation for obtaining *composite bars* in CFD [18]. To this end, a thorough analysis of the numerical error (including a quantitative assessment of the convergence order) would help estimate the additional source of error due to numerics, which should be factored in the final UQ.

The surrogate model was built using Gaussian quadrature rules for estimating PC coefficients. Although some comparison with the regression technique and Monte Carlo was provided, direct study of nested versus Gaussian quadrature rules, as well as quadrature approximation versus least-squares approach should be conducted in future works. In addition, it is recommended to use locally-

supported piecewise polynomial spaces to further reduce the computational cost of the UQ study.

All the UQ analysis was conducted using the newly developed QUTE software package (see Appendix A).

In addition to the UQ work, preliminary work on stress analysis has been conducted. A new thermoelastic stress analysis solver has been developed and validated within the FEniCS finite element framework. Preliminary findings suggest the stresses due to the thermal transient would be approaching the yield criteria of many common steels. Additional analysis of thermal cycling, and the impact this has on thermal fatigue is ongoing work.

Bibliography

[1] C AISC. *Steel Construction Manual*. American Institute of Steel Construction, 2005.

[2] Martin S Alnæs et al. "The FEniCS project version 1.5". In: *Archive of Numerical Software* 3.100 (2015), pp. 9–23.

[3] Maarten Arnst, Roger Ghanem, and Christian Soize. "Identification of Bayesian posteriors for coefficients of chaos expansions". In: *Journal of Computational Physics* 229.9 (2010), pp. 3134–3154.

[4] F. AUGUSTIN et al. "Polynomial chaos for the approximation of uncertainties: Chances and limits". In: *European Journal of Applied Mathematics* 19.2 (2008), 149–190.

[5] Stefano Conti and Anthony O'Hagan. "Bayesian emulation of complex multi-output and dynamic computer models". In: *Journal of statistical planning and inference* 140.3 (2010), pp. 640–651.

[6] Josef Dick, Frances Y Kuo, and Ian H Sloan. "High-dimensional integration: the quasi-Monte Carlo way". In: *Acta Numerica* 22 (2013), pp. 133–288.

[7] Valentina Dolci and Renzo Arina. "Proper orthogonal decomposition as surrogate model for aerodynamic optimization". In: *International Journal of Aerospace Engineering* 2016 (2016).

[8] David L Donoho et al. "Compressed sensing". In: *IEEE Transactions on information theory* 52.4 (2006), pp. 1289–1306.

[9] EDF. *Code_Saturne*. https://www.code-saturne.org.

[10] Jonathan Feinberg and Hans P Langtangen. "Chaospy: An open source tool for designing methods of uncertainty quantification". In: *Journal of Computational Science* 11 (2015), pp. 46–57.

[11] Jasmine Foo and George E Karniadakis. "Multi-element probabilistic collocation method in high dimensions". In: *Journal of Computational Physics* 229.5 (2010), pp. 1536–1557.

[12] Marc Gerritsma et al. "Time-dependent generalized polynomial chaos". In: *Journal of Computational Physics* 229.22 (2010), pp. 8333–8363.

[13] Michael B Giles. "Multilevel Monte Carlo methods". In: *Monte Carlo and Quasi-Monte Carlo Methods 2012*. Springer, 2013, pp. 83–103.

[14] Max Gunzburger, Clayton G Webster, and Guannan Zhang. "An adaptive wavelet stochastic collocation method for irregular solutions of partial differential equations with random input data". In: *Sparse Grids and Applications-Munich 2012*. Springer, 2014, pp. 137–170.

[15] SH Hashemi. "Strength–hardness statistical correlation in API X65 steel". In: *Materials Science and Engineering* 528.3 (2011), pp. 1648–1655.

[16] Serhat Hosder, Robert Walters, and Michael Balch. "Efficient sampling for non-intrusive polynomial chaos applications with multiple uncertain input variables". In: *48th AIAA/ASME/ASCE/AHS/ASC Structures, Structural Dynamics, and Materials Conference*. 2007, p. 1939.

[17] Nicolas Jarrin et al. "A synthetic-eddy-method for generating inflow conditions for large-eddy simulations". In: *International Journal of Heat and Fluid Flow* 27.4 (2006), pp. 585–593.

[18] George E Karniadakis. "Toward a numerical error bar in CFD". In: *Journal of Fluids Engineering* 117.1 (1995), pp. 7–9.

[19] OM Knio and OP Le Maitre. "Uncertainty propagation in CFD using polynomial chaos decomposition". In: *Fluid dynamics research* 38.9 (2006), p. 616.

[20] Oliver P Le Maıtre et al. "Uncertainty propagation using Wiener–Haar expansions". In: *Journal of computational Physics* 197.1 (2004), pp. 28–57.

[21] Xiaoyu Liu and Serge Guillas. "Dimension reduction for Gaussian process emulation: An application to the influence of bathymetry on tsunami heights". In: *SIAM/ASA Journal on Uncertainty Quantification* 5.1 (2017), pp. 787–812.

[22] Hung V Ly and Hien T Tran. "Modeling and control of physical processes using proper orthogonal decomposition". In: *Mathematical and computer modelling* 33.1-3 (2001), pp. 223–236.

[23] Rémi Manceau and Kemal Hanjalić. "Elliptic blending model: A new near-wall Reynolds-stress turbulence closure". In: *Physics of Fluids* 14.2 (2002), pp. 744–754.

[24] Michael D McKay, Richard J Beckman, and William J Conover. "Comparison of three methods for selecting values of input variables in the analysis of output from a computer code". In: *Technometrics* 21.2 (1979), pp. 239–245.

[25] Arash Mohammadi and Mehrdad Raisee. "Efficient uncertainty quantification of stochastic heat transfer problems by combination of proper orthogonal decomposition and sparse polynomial chaos expansion". In: *International Journal of Heat and Mass Transfer* 128 (2019), pp. 581–600.

[26] Nathan E Owen et al. “Comparison of surrogate-based uncertainty quantification methods for computationally expensive simulators”. In: *SIAM/ASA Journal on Uncertainty Quantification* 5.1 (2017), pp. 403–435.

[27] Mohammad Mahdi Rajabi. “Review and comparison of two meta-model-based uncertainty propagation analysis methods in groundwater applications: polynomial chaos expansion and Gaussian process emulation”. In: *Stochastic Environmental Research and Risk Assessment* (2019), pp. 1–25.

[28] Pamphile T Roy et al. “Comparison of polynomial chaos and Gaussian process surrogates for uncertainty quantification and correlation estimation of spatially distributed open-channel steady flows”. In: *Stochastic environmental research and risk assessment* 32.6 (2018), pp. 1723–1741.

[29] Pamphile T Roy et al. “Resampling strategies to improve surrogate model-based uncertainty quantification: Application to LES of LS89”. In: *International Journal for Numerical Methods in Fluids* 87.12 (2018), pp. 607–627.

[30] Saeed Salehi et al. “Efficient uncertainty quantification of stochastic CFD problems using sparse polynomial chaos and compressed sensing”. In: *Computers & Fluids* 154 (2017), pp. 296–321.

[31] Timothy J Sullivan. *Introduction to Uncertainty Quantification*. Vol. 63. Springer, 2015.

[32] Lloyd N Trefethen. “Is Gauss quadrature better than Clenshaw–Curtis?” In: *SIAM review* 50.1 (2008), pp. 67–87.

[33] PL Viollet. “Observation and numerical modelling of density currents resulting from thermal transients in a non rectilinear pipe”. In: *Journal of Hydraulic Research* 25.2 (1987), pp. 235–261.

[34] Xiaoliang Wan and George E Karniadakis. “An adaptive multi-element generalized polynomial chaos method for stochastic differential equations”. In: *Journal of Computational Physics* 209.2 (2005), pp. 617–642.

[35] Xiaoliang Wan and George Em Karniadakis. “Long-term behavior of polynomial chaos in stochastic flow simulations”. In: *Computer methods in applied mechanics and engineering* 195.41-43 (2006), pp. 5582–5596.

[36] Norbert Wiener. “The homogeneous chaos”. In: *American Journal of Mathematics* 60.4 (1938), pp. 897–936.

[37] Tien-Tsin Wong, Wai-Shing Luk, and Pheng-Ann Heng. “Sampling with Hammersley and Halton points”. In: *Journal of graphics tools* 2.2 (1997), pp. 9–24.

[38] Dongbin Xiu. *Numerical Methods for Stochastic Computations: A Apectral Method Approach*. Princeton University Press, 2010.

[39] Dongbin Xiu and George E Karniadakis. “The Wiener–Askey polynomial chaos for stochastic differential equations”. In: *Journal on Scientific Computing* 24.2 (2002), pp. 619–644.

[40] Dongbin Xiu and George Em Karniadakis. “Modeling uncertainty in flow simulations via generalized polynomial chaos”. In: *Journal of Computational Physics* 187.1 (2003), pp. 137–167.

Appendix A

Quantification of Uncertainty Toolkit for Engineering

Quantification of Uncertainty Toolkit for Engineering (QUTE) offers a framework where users can drive several complex uncertainty quantifications studies without having to master the complexities around the management of the multiple simulations and the underlying HPC resources, including computing environments and job scheduling.

The framework uses an as-a-service (aaS) design and provides a catalogue of UQ models and simulation applications/flows to chose from. The only requirement from the user is to provide a study (folder) compatible with one of flows in the catalogue, and annotate in that same case the quantity he/she wishes to do assess. The tools take care of the rest of the process, including:

- Replication of the study according to the UQ model's needs, so that each replica uses the right set of inputs compatible with the statistics used by the model;
- Selection of cluster or HPC facility where the simulations will take place, based on the dependencies and availability of the application used for the simulation;
- Migration of data from the user local computer to the designated cluster or HPC facility using the user defined assess credentials;
- Set-up of the environment, launching and monitoring for the simulation jobs;
- Retrieval of the outputs referring to the quantity affected by uncertainty analysis and presentation of the results in plot format.

This framework is under active development and full containerisation of the framework as well as of the applications invoked from back-end is underway. Such

infrastructure will enhance usability and provide the flexibility of cloud technologies, including automatic adjustment of job sizes and transparent partitions of the flow by multiple resources.

Appendix B

Surrogate models for UQ: A short overview

In this work, the polynomial chaos approach has been applied to quantify uncertainty in simulation of thermally stratified flow. As the problem under consideration had only one uncertain parameter, the choice of the method was straightforward. In polynomial chaos, by the correct choice of Q nodes and weights, the quadrature formula can be made accurate for all polynomials of degree at most $2Q-1$, and no other formula on Q nodes has higher order of accuracy. Therefore, in univariate setting, if a response function behaves like a polynomial, the nodes based on Gauss-type quadrature rules will minimise the number of necessary function evaluation. There are certain situations in which the spectral convergence is lost, e.g. in case of discontinuous responses (Gibbs' phenomenon). In addition, the Gauss quadratures don't perform well for high dimensions and in presence of singularities, e.g. $1/x$. To tackle these situations, numerous extensions/alternatives have been proposed. In the following section, we provide an overview of popular approaches to UQ and further discuss the reasoning behind the choice of the surrogate method.

Conventional approaches for tasks such as probabilistic modelling for risk analysis, sensitivity study and design optimisation are based around Monte Carlo sampling. Although it is a powerful approach, it is deemed infeasible for computationally intensive systems due to its slow convergence rate which depends on the inverse square root of the number of simulations performed. Some techniques have been introduced to alleviate the cost of the brute-force approach by applying variance reduction methods, such as stratified sampling using Latin Hypercube Sampling [24], quasi-Monte Carlo with deterministic inputs drawn from a sequence with low discrepancy [6], and sampling at different levels of numerical accuracy in multilevel Monte Carlo [13]. However, their applicability is still limited to high-dimensional problems and non-smooth integrands, for which the

Monte Carlo-based methods are still preferred solutions.

As mentioned in the report, an alternative to statistical methods for UQ are spectral expansion techniques. At their core, these are orthogonal decomposition methods, e.g. polynomial chaos (PC) or Karhunen–Loève, in which a random variable over a probability space, a quantity of interest (QoI), is expanded with respect to appropriate basis functions, e.g. polynomials, wavelets. Due to the nature of the analysis, we focus our review on non-intrusive strategies which compute/estimate spectral coefficients via a set of deterministic model solutions.

Another widely used UQ method is Gaussian process emulation (GP) which models the quantity of interest as a Gaussian random field. Both - Gaussian process regression and polynomial chaos expansion are often referred to as surrogate-based methods as they aim to build an approximate model which emulates the response of the original simulator [26]. In addition, combination of POD with interpolation of its coefficients (PODi methods) can also serve as an alternative surrogate modelling approach which is purely data-driven [22].

Polynomial chaos (or generalized Polynomial Chaos, gPC, for arbitrarily distributed random variable) originates in the engineering and applied mathematics communities, and was shown to be well suited for Computational Fluid Dynamics, see [40] and [19]. On the other hand, Gaussian process emulation is a statistical approach. However, it has also been recently applied to fluid modelling (see, e.g. [29]). It is not a trivial task to compare the listed techniques as they are based on different mathematical concepts. The particular modelling choices in constructing surrogates will have an effect on the conclusions that are drawn. One attempt at assessing Gaussian process emulator and polynomial chaos on a basic level, without the consideration of more advanced variants of both methods, has been made by Owen et al. [26]. Although the authors made an effort to design a fair comparison, it can be argued that the choice of samples used for the analysis affected their assessment. Additional review has been proposed by Roy et al. [28]. The article analyses the approximation accuracy of PC and GP emulation for a model of water flow with two inputs. Moreover, Rajabi [27] looked at performance of the surrogate models in ground water applications by testing them on hypothetical problems corresponding to seawater intrusion in coastal aquifers. All the studies found that neither surrogate method clearly outperforms the other, but advantages can be gained in some cases. As an example, the work of Roy et al. [28] showed that PC was more accurate in estimating the Sobol' indices that could be directly derived from the expansion coefficients. On the other hand, GP emulators seemed to be better at estimating the multimodal probability density functions. The results of the latter review claimed that GP outperforms PC in the estimation of the response function, but in most cases assessed PC provides better accuracy in the estimation of stochastic moment and PDFs.

Numerous advanced formulations of PC and GP have been presented in the

literature. Rajabi [27] provides a review for some of these formulations and their key characteristics (in [27], see Table 3 and 4). These advanced formulations have allowed both methods to improve their efficiency, accuracy, extended them to deal with arbitrary discrete probability distributions, sparse measurements or perform better with high dimensional problems.

One of the advantages of polynomial chaos mentioned in the literature, is low-cost of computing the expansion coefficients either through quadratures or regression [26]. In contrast, fitting Gaussian process emulator can be expensive, particularly for large design sizes.

Gaussian process emulators are considered to more accurately model more complex simulator behaviours by changing the mean and covariance function. However, in case of PC, the improved convergence for non-smooth, irregular response functions can be addressed by using piece-wise smooth polynomials [11] or combining hierarchical sparse grid with locally supported bases such as wavelets [14].

One of the strong benefits of Gaussian processes is the ability to provide uncertainty information due to the distributional assumptions. Although not directly, such information can also be obtained from polynomial representation by analysing the behaviour of expansion terms. Arnst et al. [3] treats the PC coefficients as unknown random variables whose probability density function is the Bayesian posterior. It is claimed that such approach allows to quantify the impact of missing experimental information on the accuracy of expansion and predictions.

Both classical PC method and GP struggle in high-dimensional setting. In polynomial chaos, to analyse problems with multiple uncertain parameters, tensor products are used which become expensive for high input dimensions, e.g., higher than five. In such case, it is recommended to use sparse grid quadrature to elevate the computational burden [38]. In addition, the compressed sensing theory can be employed to construct the sparse representation of polynomial chaos expansion (see, e.g. [30] and [8]). Joint Gaussian emulations with dimensionality reduction methods have also been introduced [21].

Performing UQ for transient problems is challenging. The convergence failures can be overcome by using basis functions with finite support, or by decomposing the probability space of the stochastic input and solving independent local problems [35]. Another approach, that has been proposed for intrusive PC, suggests adapting the basis to a set of new random variables defined by the solution itself at certain discrete time steps [12]. Gaussian process emulation was also extended to simulations of time-evolving systems [5]

Although much effort has been devoted to application of PC and GP for uncertainty quantification studies, it is not obvious how to use POD to build surrogates. Proper orthogonal decomposition is extensively used to construct reduced order models, i.e. find a basis for the projection of the Navier-Stokes equations, filter noise and extract coherent features. The application of POD-based surrogates has

recently been applied for aerodynamic shape optimization [7]. The main idea is to perform singular value decomposition on simulation outputs related to different parameters. By interpolating the POD coefficients, solutions for unseen values can be predicted. It can be shown that POD eigenfunctions will resemble polynomial basis orthogonal with respect to a given random variable. Therefore, such approach can be seen as purely data-driven polynomial chaos expansion. POD based surrogate can be used to obtain the simulation output at a given design point or to estimate stochastic moments by performing Monte Carlo modelling.

In this work, polynomial chaos approach was used including its multi-element extension to improve the accuracy of resulting surrogates. For practical applications, some of the constraints of PC, such as moderate number of random inputs, or presence of correlation between input processes, do not pose significant problem. In case of low-dimensional parameter spaces, PC works very well, particularly for steady state. In some articles, it is even argued that, if industrial relevance is considered, PC is the best alternative, which in combination with the adaptive Gauss quadrature is a state of the art method for solving stochastic Finite Elements [4].